

QENS and INS measurements. Plastic crystals are very promising for practical refrigeration applications given that they are abundantly available, environmentally friendly and easily driven and have high performance. Our work indicates a new direction for emergent solid-state refrigeration technologies. (Reported by Shinichiro Yano)

This report features the work of Bing Li and his collaborators published in *Nature* **567**, 506 (2019).

ANSTO SIKA—Cold Neutron Triple-axis Spectrometer

- Neutron Inelastic Scattering
- Materials Science, Plastic Crystal, QENS, Caloric Effect

Reference

1. B. Li, Y. Kawakita, H. Wang, T. Kikuchi, D. Yu, S.

Yano, W. Ren, K. Nakajima, Z. Zhang, *Nature* **567**, 506 (2019).



SIKA – Cold neutron triple-axis spectrometer (with dilution fridge and magnet).

Magnetic Correlations in the Disordered Fluorite $\text{Dy}_2\text{Zr}_2\text{O}_7$

$\text{Dy}_2\text{Zr}_2\text{O}_7$ has a dynamic magnetic ground state, but not possess the spin-ice correlations seen in the chemically ordered $\text{Dy}_2\text{Ti}_2\text{O}_7$ compound. Bulk magnetic properties, specific heat and neutron diffraction support that the fluctuating Dy^{3+} spins are in a disordered, liquid-like state, which do not freeze into a canonical spin-glass.

Magnetic frustration, *i.e.* competing interactions, is common in systems of interacting degrees of freedom. As a result, exotic phenomena are often observed in these systems. The magnetic frustration can be cataloged into two major types: geometric frustration and the frustrations among the random distributed magnetic ions. The cubic pyrochlore oxides, $\text{A}_2\text{B}_2\text{O}_7$, is an ideal example of geometrically magnetic frustration because the A and B ions reside on two distinct interpenetrating lattices of corner-sharing tetrahedra. If A, B, or both are magnetic and the nearest-neighbor exchange interaction is antiferromagnetic, the system is highly geometrically frustrated. As a result, antiferromagnetically coupled classical Heisenberg spins on the pyrochlore lattice do not develop long-range order at any nonzero temperature, opening up new avenues for novel intrinsically quantum mechanical effects to emerge at low temperatures.¹ However not all the $\text{A}_2\text{B}_2\text{O}_7$ compounds crystallize into the pyrochlore structure. Some of them crystallize into the disordered fluorite structure.² The title compound is one of the examples. In the disordered fluorite structure, the metal ions randomly distribute on two interpenetrating sublattices of corner-sharing tetrahedra.

In this work J. G. A. Ramon (University de São Paulo, Brazil) and his collaborators report the bulk properties and neutron diffraction of $\text{Dy}_2\text{Zr}_2\text{O}_7$, suggesting that a significant amount of disorder can lead to a dynamic ground state when combined with frustration at low temperatures. $\text{Dy}_2\text{Ti}_2\text{O}_7$, a well-studied pyrochlore compound, is in the “spin ice state” at low temperatures. The recovered electronic entropy, shown in **Fig. 1**, asymptotically approaches $(R/2)\ln(3/2)$ which is the ice entropy found by Linus Pauling. On the other hand, the recovered entropy of $\text{Dy}_2\text{Zr}_2\text{O}_7$ is close to the $R\ln(2)$, for a system with only two discrete orientations. This directly indicates that there is no spin-ice state in $\text{Dy}_2\text{Zr}_2\text{O}_7$.

Magnetic diffraction data sets at 40 mK are shown in **Fig. 2**. The net intensity has been corrected for the $|Q|$ dependence due to the Dy^{3+} magnetic form factor so that models of possible spin structures can be compared.

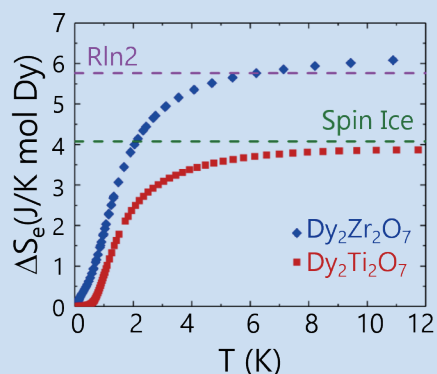


Fig. 1: Recovered electronic entropy S_e as a function of the temperature for $\text{Dy}_2\text{Zr}_2\text{O}_7$ and $\text{Dy}_2\text{Ti}_2\text{O}_7$. The dashed lines denote the expected values for Ising spins ($R\ln 2$) and spin ices. [Reproduced from Ref. 3]

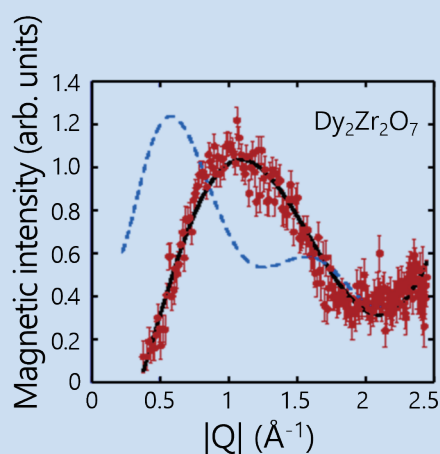


Fig. 2: Magnetic neutron scattering for $\text{Dy}_2\text{Zr}_2\text{O}_7$ at 40 mK, after a dataset at 10 K was subtracted to remove the non-magnetic background, including that from the crystalline structure. Data (red circles) are plotted against the powder-averaged dipolar spin-ice model (dashed line). [Reproduced from Ref. 3]

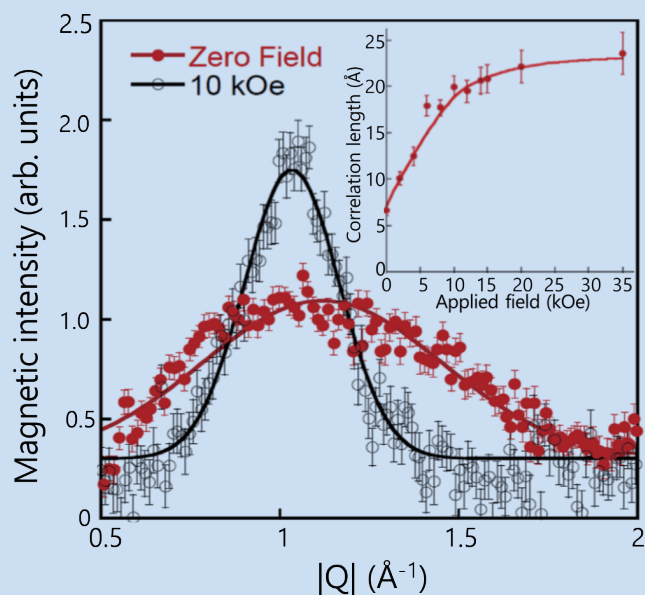


Fig. 3: Spatial spin-spin correlations as a function of the applied magnetic field at 40 mK. Main panel: Magnetic diffraction at 0 and 10-kOe Gaussian fits with a common instrumental background are used to describe the data. Inset: Field dependence of the correlation length determined from the Gaussian width of the broad maxima seen around $|Q| \approx 1.15 \text{ \AA}^{-1}$. [Reproduced from Ref. 3]

No long-range magnetic order is observed. The broad distribution of excess magnetic scattering centered at roughly 1.2 \AA^{-1} is characteristic of antiferromagnetically coupled Ising spins on the corner-sharing tetrahedral lattice. The lack of forward scattering at low $|Q|$ indicates the absence of ferromagnetic correlations and is consistent with our negative Curie-Weiss temperature. The blue dashed line represents the powder average dipolar spin-ice model observed in $\text{Dy}_2\text{Ti}_2\text{O}_7$, $\text{Dy}_2\text{Sn}_2\text{O}_7$ and the other spin-ices, where the scattering maximizes at $|Q| \sim 0.6$ and $\sim 1.6 \text{ \AA}^{-1}$, which is very different from that observed in $\text{Dy}_2\text{Zr}_2\text{O}_7$.

In the presence of magnetic field the shape of the low angle scattering visibly changed. When 10 kOe is applied, as shown in **Fig. 3**, the broad scattering sharpens up, but remains centered at $1.15(7) \text{ \AA}^{-1}$. Fitting these, and other data, results in the curve shown in the inset. Here we plot the correlation length calculated from the full width at half maximum of the broad diffuse scattering. The observed short-range, spin-spin correlations lengthen in a field, but appear to saturate above 15 kOe. This may be a plateau that extends to 35 kOe but more studies at higher fields are necessary. Within this field region the correlations extend to $23.6(8) \text{ \AA}$, the length of approximately six nearest neighbors or five unit cells.

These studies have shown that a significant amount of disorder can lead to a dynamic ground state when combined with frustration at low temperatures. Other geometrically frustrated magnets also show that disorder plays a similar role. With the availability of zirconate single crystals and the possibility of solid solution between the spin-ice and spin-liquid candidate end members, this family seems to be an excellent platform for further investigations, probing the role of extensive disorder on the spin dynamics of pyrochlores and the propagation of monopoles as disorder is induced to the Coulomb phase.

The above neutron diffraction measurements were carried out on the high-intensity neutron diffractometer, **WOMBAT** at the OPAL reactor.⁴ The pyrolytic-graphite monochromator was employed to deliver the long-wavelength neutrons (up to $\sim 5 \text{ \AA}$) which is very useful for the studies of the magnetism. The large-area position-sensitive detector of Wombat enables fast data acquisition speed. In this work counting time of ~ 1 hour per pattern is enough for 300 mg of ^{162}Dy -enriched sample. Chin-Wei Wang (NSRRC) performed all the diffraction experiments on WOMBAT and analyzed the neutron scattering data. He also collected inelastic data measurements on **SIKA** and **TAIPAN** but the data was not presented in the current paper. (Reported by Chin-Wei Wang)

This report features the work of J. G. A. Ramon and his collaborators published in *Phys. Rev. B* **99**, 214442 (2019).

ANSTO WOMBAT—High-intensity Powder Diffractometer

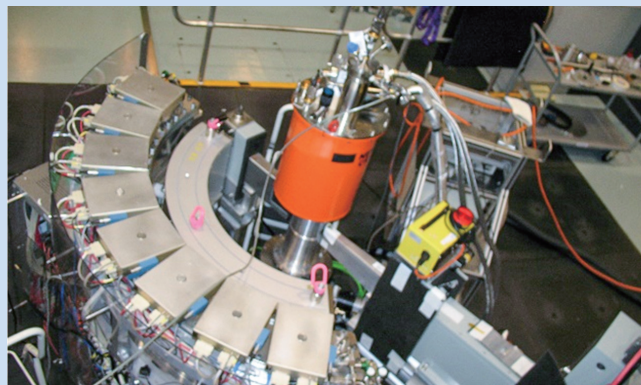
- Powder diffraction, Single Crystal Diffraction
- Materials Science, Magnetism, Condensed-matter Physics

References

1. J. S. Gardner, M. J. P. Gingras, J. E. Greedan, *Rev. Mod. Phys.* **82**, 53 (2010).
2. C. R. Stanek, C. Jiang, B. P. Uberuage, K. E. Sickafus, *Phys. Rev. B* **80**, 174101 (2009).
3. J. G. A. Ramon, C. W. Wang, L. Ishida, P. L. Bernardo, M. M. Leite, F. M. Vichi, J. S. Gardner, R. S. Freitas,

Phys. Rev. B **99**, 214442 (2019).

4. A. J. Studer, M. E. Hagen, T. J. Noakes, *Physica B* **385**, 1013 (2006).



Wombat high-intensity powder diffractometer.

How a Superbug Escape Antibiotic Attack?

The rise in antibiotic resistance represents one of the greatest threats to human health, with international organizations and governments calling for urgent action to tackle the crisis. Neutron diffraction has served in an investigation of how bacteria changes the membrane phospholipid composition to compromise antibiotic actions, which provides hints of innovative bacterial membrane-based therapies for treatment.

Dominating the list of ‘red-alert’ antibiotic resistant bacteria is methicillin-resistant *Staphylococcus aureus* (MRSA), which is well known as Golden staph. As one of the most notorious human pathogens, *S. aureus* has uncanny ability to adapt to antibiotic and host immune selection pressure, promoting bacterial survival, persistence and therapeutic failure. Treatment of severe MRSA infections increasingly relies on last-line antibiotics, including daptomycin (DAP). DAP targets bacterial cell membrane to execute its bactericidal effects and the emergence of resistance to daptomycin (DAP-R) in *S. aureus* is of serious concern. However, how *S. aureus* develop resistance is not entirely clear.

Anton Peleg’s group at Monash University, Australia, discovered that clinical MRSA isolate was able

to change its membrane phospholipid composition *via* single point mutation in the gene responsible for cardiolipin biosynthesis.¹ This compositional change of the membrane phospholipids led to daptomycin resistance. To further investigate the mechanism of resistance, membrane bilayers mimicking DAP-R MRSA membrane were reconstituted and Chun-Ming Wu (NSRRC) utilized the advantages of neutrons as a probe to analyze the structural changes on membrane bilayers caused by daptomycin.

Figure 1 shows the profiles of small-angle neutron scattering (SANS) of membrane bilayers. Synthetic phosphatidylglycerol, cardiolipin and lysyl-phosphatidylglycerol were dissolved in chloroform and mixed at the molar ratios of 69:12:19 and 23:60:17 for

DAP-sensitive and DAP-R membranes respectively. The lipid mixtures were dried under nitrogen and resuspended in HEPES buffer (5mM CaCl₂, 150mM NaCl, 10mM HEPES, pH 7.4) with D₂O using a water bath sonicator. Daptomycin was added to the membrane suspension and the mixtures were transferred to Hellma cuvettes (Hellma Analytics, Germany). The samples were measured using the SANS instrument, **QUOKKA**, at ANSTO over a Q range of ~ 0.02 – 0.21 \AA^{-1} where $Q = 4\pi/\lambda \cdot \sin\theta$, with $\lambda = 5 \text{ \AA}$, $\Delta\lambda/\lambda = 10\%$ resolution and the scattering angle 2θ , providing a length scale of 3–31.4 nm. The distances of source-to-sample (L1) and sample-to-detector (L2) were 4 meters, with source and sample apertures of 50 mm and 5 mm in diameter respectively. The data were reduced using SANS reduction macros developed at